Journal of Thermal Analysis and Calorimetry, Vol. 91 (2008) 1, 93–100

KINETICS OF REDUCTION OF SUPPORTED NANOPARTICLES OF IRON OXIDE

Claudia Messi[1], *P. Carniti*[1] *and Antonella Gervasini*[1,2]*

[1]Dipartimento di Chimica Fisica ed Elettrochimica, Università degli Studi di Milano, via C. Golgi n. 19, 20133 Milano, Italy
[2]Centro di Eccellenza CIMAINA, Università degli Studi di Milano, via C. Golgi n. 19, 20133 Milano, Italy

A series of catalysts prepared by dispersing iron oxide on supports of different nature and acidity has been studied. Silica (S) and silica-zirconia mixed oxides (SZ) with different ZrO_2 content (from 5 to 45 mass%) were used as supports for the iron oxide phase which was deposited over them by an equilibrium-adsorption method. The red-ox properties of the Fe-catalysts were studied by temperature programmed reduction (TPR) technique.

The two well defined and narrow TPR peaks observed could be associated with the reduction steps: I) $Fe_2O_3 \rightarrow FeO$ and $Fe_2O_3 \rightarrow Fe(0)$ (at ca. 400°C) and II) $FeO \rightarrow Fe(0)$ (at ca. 800–900°C). The temperature of the second-step-peak increased with the zirconia content in the support, likely because of the stronger interaction of the iron oxide phase with the support. Activation parameters for the two step-reduction processes were obtained by a simple computation procedure applied to the TPR profiles.

Keywords: *iron oxide, kinetics of reduction, supported catalysts, temperature programmed reduction*

Introduction

Thermal analysis techniques are widely used in catalysis for various characterisation analyses of catalytic solids and surfaces. Among these, temperature programmed reduction (TPR) analysis has found great success not only for studying the reducing properties of active metal phases but also for collecting information on the dispersion and aggregation state of supported phases. Qualitative (shape and position of TPR peaks) and quantitative (amount of reducible gas consumed) data provide very useful information on the metal phase in terms of nature and dispersion. Therefore, TPR technique has been recognized as an important tool in the research aimed at characterizing both the bulk and dispersed metal phases [1–7].

Recently, supported iron oxide catalysts have received much attention because their potentiality for many applications in environmental catalysis (N_2O decomposition and reduction) [8, 9] and in fine chemical industry for reactions requiring strong Lewis acid sites (Friedel-Crafts, isomerisations, etc.) [10, 11]. For most catalytic applications, high dispersion of the metal centers is desirable to enhance the activity-selectivity pattern of the catalyst. Conventional methods used to disperse metal centers in silica structures (zeolites, MCM, SBA, etc.) exploit the ionic exchange properties of the support substrates [12–14]. A completely different situation is present when an oxide is concerned as substrate. In this case, the low number of exchangeable sites does not allow to exploit the same preparation methods. The formation of highly dispersed and nanosized iron oxide aggregates on oxide supports is then a very difficult task. For this purpose, different synthetic approaches and Fe-precursors of the iron oxide phase have been tested [15–18].

In this work, we present the study performed on a series of catalysts constituted of a supported iron oxide phase over oxide supports of varying nature and acidity. The supported iron phase was deposited by an adsorption equilibrium method, already use for the preparation of copper-based catalysts [19, 20]. It is known that the properties of the dispersed phases are dependent on the interaction with the relevant support. The supported iron oxide phase can then have some properties, in particular the red-ox properties and metal dispersion, influenced by the support nature. TPR was chosen as thermal analysis technique to investigate on the reducibility of the variously supported iron oxide. The reducing profiles of the iron-catalysts have been evaluated from quantitative point of view and kinetically interpreted to obtain the activation parameters of the reaction of iron oxide reduction. Strong influence of the support nature and properties have been observed on the path followed by the dispersed iron oxide for the reduction to metal iron.

* Author for correspondence: antonella.gervasini@unimi.it

1388–6150/$20.00

Akadémiai Kiadó, Budapest, Hungary
Springer, Dordrecht, The Netherlands

Table 1 Catalyst presentation with their main properties

Sample code	Composition/mass%			Surface area/m^2 g^{-1}	Pore size[a]/nm
	SiO_2	ZrO_2	Fe_2O_3		
Fe/S	92.74	0	7.26	239.2	7
Fe/SZ-5	89.44	4.71	5.85	237.4	4
Fe/SZ-15	80.21	14.16	5.63	231.5	4
Fe/SZ-30	65.56	28.09	6.35	298.1	4
Fe/SZ-45	52.62	43.05	4.33	237.5	4
Fe/SZ-5(w.i.)[b]	84.51	4.45	11.04	224.0	4

[a]main population of pore size calculated from B.J.H. [33], [b]catalyst prepared by wetness impregnation (w.i.)

Experimental

Materials

Iron catalysts were prepared from Fe(III)-acetyl-acetonate precursor, adsorbing it on the supports suspended in a water/propanol solution. As supports, a pure silica (S) and a series of silica-zirconia oxides (SZ) (containing from 5 to 45 mass% of ZrO_2) prepared by sol-gel route were used. After filtration, drying, and calcination (500°C), orange solids containing Fe in an amount of 4–5 mass% were obtained (Table 1). For comparative purpose, a conventional Fe-catalyst was prepared by wetness impregnation (w.i.) starting from $Fe(NO_3)_3$ precursor and SZ-5 as support.

The iron content of the samples were measured by ionic exchange chromatographic analysis after solid dissolution in acid mixtures and reaction in a microwave digestor at 220°C. The composition of each sample is reported in Table 1, expressed as mass% of Fe_2O_3, SiO_2 and ZrO_2 oxides.

Methods

Catalyst characterization for the determination of the structure, by XRD, morphology, by N_2 adsorption-desorption isotherms and SEM, electronic properties by DR-UV, EPR, and XPS spectroscopies, acid properties, by TPD of basic probe, was performed and results will be presented elsewhere [20].

Pure Fe_2O_3, Fe_3O_4, and FeO (Aldrich, purity >99.9%) powders were used as reference samples for the analyses of reduction under programmed heating rate.

Reduction experiments in isothermal and temperature programmed heating conditions

Reduction analyses in programmed temperature (TPR) and/or isothermal conditions were realized on freshly oxidized samples (350°C for 1 h under air flowing, 45 mL min^{-1}). A TPDRO–1100 (Thermo Electron Corporation) equipped with a quartz reactor with porous septum (ca. 8 mm i.d.) and a filter filled with soda lime for trapping acid gases and water was employed. TPR measurement was carried out using H_2/Ar (5.03% v/v) as reducing gas mixture. The gas flow rate was adjusted by mass flow controllers to 15 cm^3 min^{-1}. A thermal conductivity detector (TCD) measured the amount of H_2 uptake. The obtained TPR peaks were integrated for quantitative determination of H_2 consumed. Calibrations for the determination of H_2-consumption were performed by both CuO bulk standard per analysis as reference material and pure H_2 (Sapio, Italy; purity >99.9999%) injections.

Conventional TPR runs forecast a first heating step from 50 to 1000°C (typical heating rate, 8°C min^{-1}) followed by an isothermal step at 1000°C for 2 h. Sample size used (ca. 0.07 g sieved between 45–60 mesh) corresponded to about 30 μmol of Fe_2O_3; this allowed to maintain *K* and *P* values [21, 22] around 70 s and 10°C, respectively, for all the analyses. Pure iron oxides (Fe_2O_3, Fe_3O_4 and FeO), used as reference materials, were mixed with silica sand to obtain mixture containing 4–6 mg of reducible oxide in 100 mg of sand.

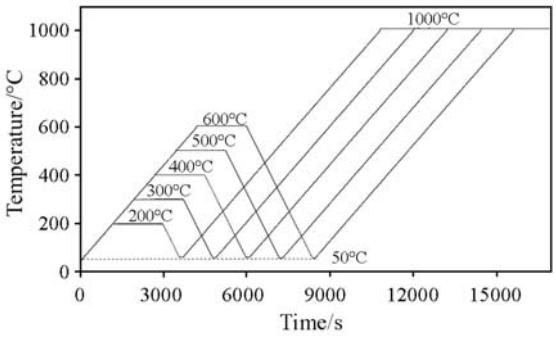

Scheme 1 Thermal programme used for the reduction experiments in isothermal conditions (from 300 to 600°C) followed by temperature programmed analyses (from 50 to 1000°C)

On selected samples, a series of isothermal reductions under H_2/Ar flowing (5.03% v/v) performed at defined temperature, starting from the lowest at 200°C to the higher ones (300, 400, 500 and 600°C) each one maintained for 0.5 h, were carried out. After each isothermal pre-reduction, the samples, cooled to 50°C in inert flowing atmosphere (Ar, 20 mL min^{-1}), were further reduced under programmed temperature (TPR) from 50 to 1000°C, maintaining the final temperature for 1 h only (Scheme 1). The sample mass, and TPR conditions were analogous to those above reported.

Kinetic computation

The conventional TPR profiles (TCD signal, mV g^{-1}, *vs.* analysis time, s) were divided into very small constant intervals (Δt=1 s) which were integrated obtaining the H_2 consumption value for each interval. The obtained H_2 consumption values were summed each other to obtain a curve describing the total H_2 consumed as a function of analysis time or temperature. On each curve, the zones of exponential increase of the H_2 consumption *vs.* analysis time were numerically treated to obtain the Arrhenius activation parameters.

Results and discussion

The studied samples comprised an oxide support (silica and mixed silica-zirconias with variable amount of zirconia) and an iron oxide supported phase. Composition and main morphologic properties are listed in Table 1. The adsorption equilibrium method used to deposit the iron phase on the supports guaranteed the obtainment of highly dispersed iron aggregates that, after calcination, gave dispersed iron oxide nanophases. The diffractometric analysis (XRD) did not show any line, indicating the total amorphous character of both the support and iron oxide phases and the presence of aggregates of iron oxides of nanometric dimensions below the limit of detection of XRD.

The spectrophotometric (XPS) and spectroscopic (DRS-UV) analyses [23] converged on the identification of the nature of the iron phase. Over all the surfaces, binding energy in the 710.9–711.7 eV interval (Fe $2p_{3/2}$) was diagnostic of the Fe_2O_3 presence. UV-bands with maxima at ca. 400–500 and 330–350 nm, typical of nanosized Fe_2O_3 particles with dimension around 5 nm and of lower nuclearity Fe-oxide particles, were observed, respectively.

The catalyst prepared by impregnation gave well visible, even if not much intense, diffraction peaks, typical of the presence of Fe_2O_3 crystalline aggregates (35.6, 44.2, 63.2° 2θ) of about 130 Å of dimension.

Temperature programmed reduction (TPR) analyses

Much work has been performed on the reducibility of bulk iron oxides under linear heating rate (TPR) and isothermal conditions [24–26]. Analysis by TPR furnishes the fingerprint of the reduction of each oxide showing one or more peaks with/without shoulders with well defined positions of the peak maxima of reduction (T_{max}). Moreover, quantitative results on the amount of reductant (e.g., H_2) consumed during the reduction complement the information for the determination of the iron oxide nature.

Reduction of pure hematite by hydrogen is a complex event that can proceed in different steps via intermediate oxides (i.e., magnetite, Fe_3O_4, and wüstite, FeO_x). The possible reduction reactions, involving hematite and the other derived oxides, have been written here below. The reduction to metal iron can occur by a reaction sequence or by a one single reduction step; each step has a defined molar ratio among the oxide, reductant, and product:

(i) $Fe_2O_3 + 3H_2 \rightarrow 2Fe + 3H_2O$

(ii) $3Fe_2O_3 + H_2 \rightarrow 2Fe_3O_4 + H_2O$

(iii) $3Fe_2O_3 + 3H_2 \rightarrow 6FeO + 3H_2O$

(iv) $Fe_3O_4 + 4H_2 \rightarrow 3Fe + 4H_2O$

(v) $Fe_3O_4 + H_2 \rightarrow 3FeO + H_2O$

(vi) $(1–x)Fe_3O_4 + (1–4x)H_2 \rightarrow 3Fe_{(1–x)}O + (1–4x)\,H_2O$

(vii) $FeO + H_2 \rightarrow Fe + H_2O$

(viii) $Fe_{(1–x)}O + H_2 \rightarrow (1–x)Fe + H_2O$

Generally, the first step in the hematite reduction is the formation of Fe_3O_4. Accordingly, observation of a TPR peak at low temperature (the exact position diverges to a large extent dependent on impurities) corresponds to the Fe_3O_4 formation. Our experimental results confirmed those of the literature; TPR of pure Fe_2O_3 powder showed one first peak at low temperature (370°C) followed by a principal peak with maximum at 550°C. Reduction (TPR spectrum integration gave 100% reduction) likely passed through the (*ii*) and (*iv*) reduction steps. The Fe_3O_4 reduction profile gave one symmetrical peak with T_{max} at 550°C, while the reduction of FeO was observed at very higher temperature (797°C). Quantitative reductions could be calculated for Fe_3O_4 (step *iv*) and FeO (step *vii*), too.

A very different and complex situation occurs when supported iron phases were concerned. Complex reduction patterns are usually observed because of the presence of mixtures of iron oxides, promoters, different sizes of oxide aggregate, and development of oxide-support interaction [27–30]. On such convo-

Table 2 Quantitative results obtained from TPR analyses of the Fe-catalysts

Sample code	$T_{max,1}$/°C	$T_{max,2}$/°C	H_2 consumed/μmol g^{-1}				I-TPR peak ($T_{max,1}$)[b]/%		II-TPR peak ($T_{max,2}$)[c]/%
			Total		Partial		Path A	Path B	
			Calc.[a]	Exp.	$T_{max,1}$[b]	$T_{max,2}$[c]	$Fe_2O_3 \rightarrow FeO$	$Fe_2O_3 \rightarrow Fe$	$FeO \rightarrow Fe$
Fe/S	420	800	1364.8	1386.8	590.0	819.2	29.6	9.8	59.1
Fe/SZ-5	420	780	979.4	1080.2	512.6	550.8	25.5	14.1	51.1
Fe/SZ-15	420	900	1058.1	1071.2	638.5	432.9	20.2	24.4	40.4
Fe/SZ-30	430	900	1192.5	1103.4	569.5	534.1	22.4	32.8	44.8
Fe/SZ-45	450	900	1001.9	824.4	481.3	353.8	17.6	46.9	35.4
Fe/SZ-5(w.i.)	371–510	671–785	2073.5	2397.8	n.d.	n.d.	n.d.	n.d.	n.d.

[a] $Fe_2O_3 + 3H_2 \rightarrow 2Fe + 3H_2O$; [b] $Fe_2O_3+H_2 \rightarrow 2FeO$ (path A) *plus* $Fe_2O_3+3H_2 \rightarrow Fe+3H_2O$ (path B); [c] $FeO+H_2 \rightarrow Fe+H_2O$

luted profiles, the identification of the reduction path followed by iron oxide is not an easy task. The TPR profile of the catalyst prepared by impregnation, Fe/SZ-5(w.i.), gave a convoluted curve (Fig. 1) that resembled those reported in the literature for the shape of the curve and temperatures of the reduction peaks [27, 28]. Comparing the reduction peak temperatures (Table 2) with those observed for the iron oxide standard samples, it is possible to guess the reduction path followed by the iron oxide phase. The reduction of Fe_2O_3 to Fe(0) proceeded through Fe_3O_4 (T_{max} at 371 and 510°C) and FeO (T_{max} at 785°C) intermediates. Because FeO should not be present on the fresh surface of Fe/SZ-5(w.i.), it had to be formed from a more oxidized Fe-phase. Reduction steps (*iii*) and (*v*) are relevant to Fe_2O_3 and Fe_3O_4 reduction to FeO; one of these reactions could be responsible of the TPR peak observed at 671°C. The complexity of the TPR profile of Fe/SZ-5(w.i.) reveals the high heterogeneity of the iron surface in terms of nature of the oxides, dimension of oxide aggregates, and oxide-support interaction.

A completely different situation emerges when TPR profiles of the Fe-catalysts prepared by adsorption method are examined (Fig. 2). All the spectra are dominated by two well defined and intense peaks positioned at low ($420<T_{max,1}/°C<450$) and high ($780<T_{max,2}/°C<900$°C) temperatures. The position of the low temperature peak was lightly affected by the nature of the support; only a light shift at higher temperature can be noticed by increasing the zirconia content in the support ($T_{max,1}$ of Fe/SZ-30 and Fe/SZ-45, Table 2). The position of the high temperature peak ($T_{max,2}$) was comprised in a large interval and the value depended on the support nature. For the catalysts prepared on silica and on silica-zirconia at lowest zirconia content (Fe/S and Fe/SZ-5), $T_{max,2}$ was around 800°C. On the contrary, for the catalysts prepared on the supports with higher zirconia content (Fe/SZ-15, Fe/SZ-30 and Fe/SZ-45), $T_{max,2}$ was around 900°C. Integration of the TPR spectra indicated complete reduction of iron oxide (Fe_2O_3 to Fe) in any case, as shown by the comparison between the calculated and experimental H_2 consumed (Table 2), but Fe/SZ-45 for which a reduction of 82% could be calculated. The two well defined and sharp reduction peaks of the Fe-catalysts prepared by the adsorption method suggest that iron oxide aggregates were of very smaller dimension than those of impregnated catalyst. Moreover, the shift at higher temperatures of the FeO reduction peak suggests that a strong metal oxide-support interaction was active when zirconia was concerned.

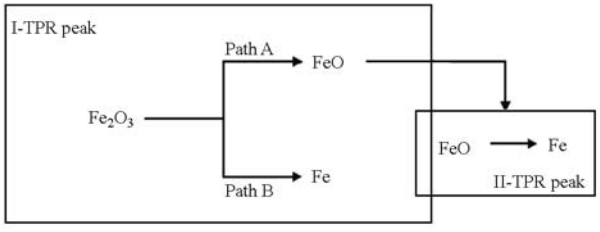

Scheme 2 Proposed reduction path for the supported iron species prepared by equilibrium adsorption method according to TPR results

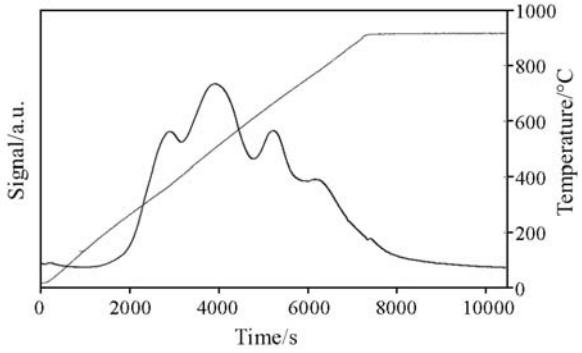

Fig. 1 TPR profile of Fe/SZ-5(w.i.) sample collected at 8°C min^{-1} from 50 to 1000°C under H_2/Ar (5% v/v) flowing

Table 3 Quantitative results of the reduction experiments in isothermal conditions followed by temperature programmed (TPR) analyses of the Fe/S and Fe/SZ-30 samples

Sample	Isothermal reduction		TPR					Σ(isothermal+ TPR)
	T/°C	Red./%	T_{max1}/°C	T_{max2}/°C	Red.$T_{max,1}$/%	Red.$T_{max,2}$/%	Red./%	Red./%
Fe/S	200	<2	420	780	52.0	48.0	93.7	93.7
	300	3.9	420	780	47.5	53.4	97.3	102.2
	400	22.0	420	780	37.5	62.5	73.4	95.5
	500	40.4	440	780	22.7	77.3	57.2	97.6
	600	45.2	460	780	9.1	90.9	50.8	96.0
Fe/SZ-30	300	4.2	420	900	53.2	46.8	97.6	101.4
	400	22.3	420	900	41.4	58.6	74.4	96.7
	500	45.5	420	920	19.3	80.7	57.5	102.9
	600	51.7	410	920	18.9	81.1	56.0	107.7

Separate quantification of the H_2-consumption of the two TPR peaks gave information on the reduction path of the supported iron oxide, under the assumption that Fe_2O_3 was the sole phase present in the catalyst samples. A simple-two-step-reduction path ($Fe_2O_3 \rightarrow FeO \rightarrow Fe$, reduction steps *iii* and *vii*) did not hold, on the basis of the quantitative data of H_2 consumption and the amount of iron present in the catalysts. The high temperature reduction peak (II-TPR peak) could be doubtless assigned to the FeO reduction (step *vii*), due to the $T_{max,2}$ value. From the H_2 consumption of II-TPR peak, it was possible to know the amount of FeO reduced and that of the parent Fe_2O_3 phase (step *iii*). From the stoichiometric computations, it was found that the amount of Fe_2O_3 present in each sample was superior than that necessary for the FeO formation. This signified that a part of Fe_2O_3 should be reduced by a different path, likely leading directly to metallic iron from hematite phase (step *i*). Scheme 2 reports our proposed reduction path for the supported iron oxide phase on the basis of the quantitative evaluation of H_2-consumption. In this case, Fe_3O_4 formation has not been clearly detected, as in the case of the impregnated Fe-catalyst (presence of the peak at 370°C). An inspection of Table 2 reveals that the II-TPR peak regularly decreased with the increase of zirconia content in the support. In parallel, the direct formation of metallic iron from hematite (path B of the I-TPR peak) regularly increased

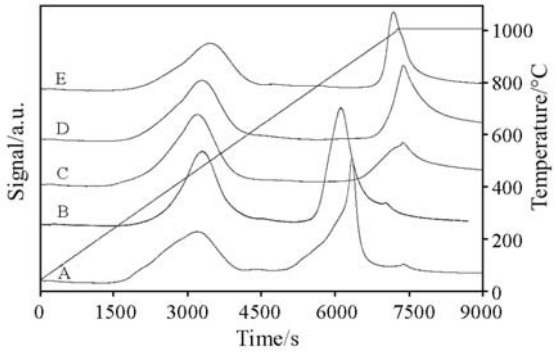

Fig. 2 TPR profiles of A – Fe/S; B – Fe/SZ-5; C – Fe/SZ-15; D – Fe/SZ-30; E – Fe/SZ-45 samples collected at 8°C min^{-1} from 50 to 1000°C under H_2/Ar (5% v/v) flowing

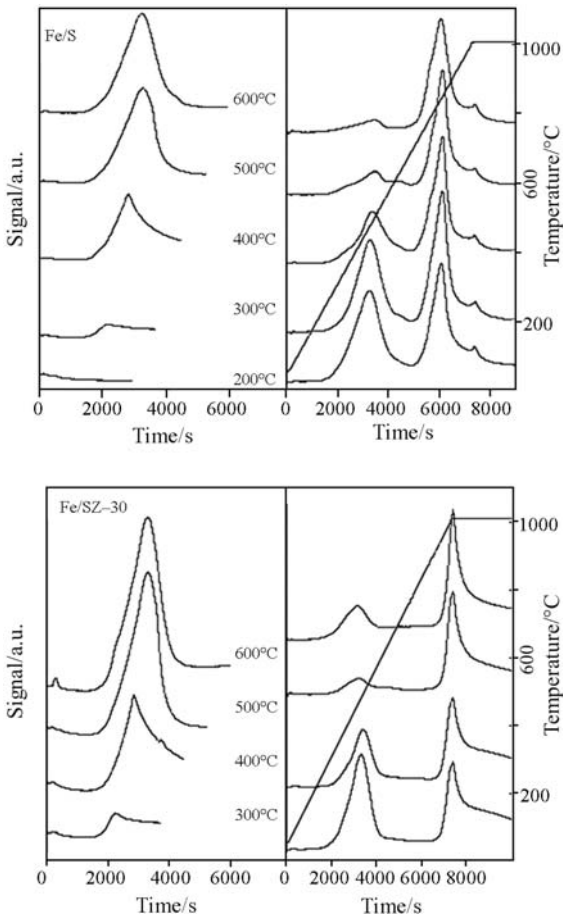

Fig. 3 Reduction experiments in isothermal conditions (from 300 to 600°C) (left side) followed by temperature programmed analyses (from 50 to 1000°C) (right side) for Fe/S and Fe/SZ-30 samples

Table 4 Kinetic results obtained from the TPR analyses of the Fe-catalysts (heating rate, 8°C min^{-1})

Sample code	I-TPR peak				II-TPR peak			
	ln A/s	E_a/kJ mol^{-1}	r	$k_{(450°C)}$/s	ln A/s^{-1}	E_a/kJ mol^{-1}	r	$k_{(850°C)}$/s^{-1}
Fe/S	1.853	47.7	0.999	0.0023	27.542	292.7	0.993	0.0223
Fe/SZ-5	2.932	52.3	0.999	0.0032	44.148	428.0	0.999	0.1851
Fe/SZ-15[a]	4.494	62.0	0.999	0.0030	42.671	466.6	0.996	0.000682
Fe/SZ-30	5.249	65.4	0.999	0.0035	89.943	913.7	0.998	0.000372
Fe/SZ-45	3.195	57.4	0.999	0.0017	95.612	977.2	0.996	0.000119

[a]E_a values of 60.6 (ln$A$ of 4.138) and 65.5 (ln$A$ of 5.173) kJ mol^{-1} for heating rate of 5 and 12°C min^{-1}, respectively for the I-TPR peak

with the zirconia content in the support. It can be inferred that support surfaces richer in zirconia promoted the Fe_2O_3 reduction by a different path that silica without the intermediate formation of the metastable FeO_3 phase.

For an in depth study of the reducibility of the supported iron phase, other reduction experiments were carried out on selected samples. Fe/S and Fe/SZ-30 were chosen as representative samples due to the very large difference in the support composition. After complete oxidation of their surfaces, they were first isothermally reduced in the temperature range from 200 to 600°C, then cooled to 50°C and reduced again with programmed heating rate (TPR) to 1000°C (Scheme 1). When the isothermal temperature of reduction was low (200 and 300°C), the TPR spectra obtained were very similar to those of Fig. 2. For isothermal reductions at higher temperatures (400–600°C), besides a well evident pre-reduction (Fig. 3 (left side) and Table 3), modified TPR spectra were obtained. The I-TPR peak regularly decreased with increasing isothermal reduction temperature, as expected (Table 3). It is interesting to note that the calculated amount of FeO reduced in the II-TPR peak, deriving from the parent Fe_2O_3 phase, was constant in all the experiments (around 47% and 45% for Fe/S and Fe/SZ-30, respectively). This indicated that the formation of the metastable FeO phase was not affected by the thermal history of the sample but it depended on the nature of the support on which the parent Fe_2O_3 was stabilized. This conclusion is in contrast with the literature results indicating that the reduction path and intermediate formed during bulk Fe_2O_3 reduction are dependent on reduction temperature [24]. In the case of the supported Fe_2O_3 phase, the development of metal-support interaction predominates over the massive oxide interaction.

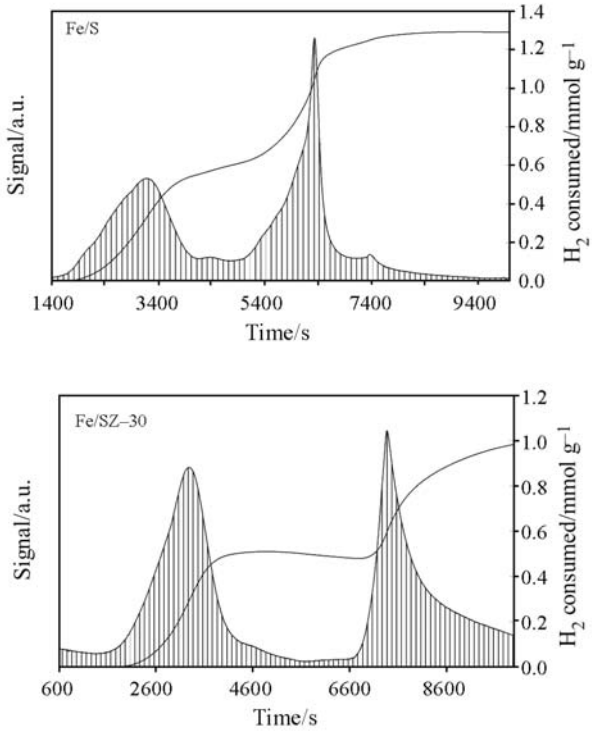

Fig. 4 Examples of TPR peak integration; the obtained curve of H_2 consumption as a function of analysis time (right axis) is drawn

Kinetic analysis

The kinetics of reduction of supported iron oxides is an important point that deserves investigation. There are numerous models in the literature for the estimation of the kinetic parameters for the reduction of oxidic species based on nucleation model or contracting sphere model [1, 2, 27, 30–32]. Some of them make use of the well-known correlation describing the shift in T_{max} with the heating rate while other are based on peak-shape analysis.

In this study, the kinetic analysis to obtain the activation parameters was performed applying a classical Arrhenius plot by using a peak-shape analysis of the data reported in Fig. 2.

The reduction reaction of the supported Fe_2O_3 phase can be described by the rate equation of the type:

$$\text{rate} = k\,[Fe_2O_3] \quad (1)$$

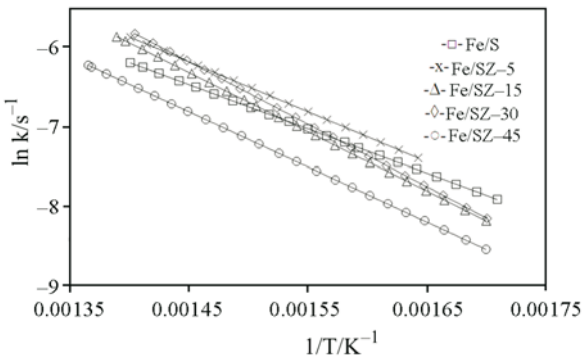

Fig. 5 Arrhenius plot for the I-TPR peak reduction of the Fe-catalysts

where [Fe_2O_3] is the actual concentration at any reaction time and k is the rate constant. Equation (1) makes use of first order with respect to reducible solid phase and zero order in H_2 concentration, in agreement with some authors [2].

The classical Arrhenius dependence on temperature for k can hold,

$$\ln k = \ln A - E_a/RT \quad (2)$$

where E_a is the activation energy and A the Arrhenius pre-exponential constant.

Firstly, a graphical procedure was made, as shown in Fig. 4, as an example. The TPR spectrum was divided in small portions (Δt=1 s) that were integrated to obtain the amount of H_2 consumed in each time interval. Summing all the integrated portions, the curve of total H_2 consumption as a function of reaction time was obtained. In the time interval correspondent to the ascending I-TPR and II-TPR peaks, section of exponential curves could be observed (Fig. 4). For each point of these portions of curve, the rate was evaluated and the rate constant was calculated by Eq. (1). Because each calculated rate constant was related to a defined temperature, the classical Eq. (2) was applied to obtain the activation parameters. Arrhenius plot for the I-TPR peaks of all the catalysts is shown in Fig. 5. The obtained kinetic results are collected in Table 4. In the Table are also reported the rate constants calculated at 450°C (for the I-TPR peak) and at 850°C (for the II-TPR peak). The obtained kinetic parameters are not affected by the condition used in the TPR analysis. On Fe/SZ-15, TPR data were collected at 5, 8 and 12°C min^{-1} of heating rate and the values of the calculated activation parameters did not vary significantly.

The E_a values for the I-TPR peak are comprised in a narrow interval (48–65 kJ mol^{-1}) with mean value of 57 kJ mol^{-1}. This suggests that there is not a great difference in the dimension and aggregation state of the Fe_2O_3 phase among the different samples. On the contrary, the E_a values of the II-TPR peak vary in a very large interval passing from 293 (Fe/S) to 977 (Fe/SZ-45) kJ mol^{-1}. Once again, the influence of the zirconia content in the support affects the reducibility of the iron oxide-phase (FeO). Likely on zirconia, the FeO interaction is stronger than on SiO_2 and higher activation energy is necessary for its reduction.

Conclusions

Temperature programmed reduction was successfully used for the study of the reducing properties of supported iron oxide phases. The reducing path of hematite was found to be dependent on the support; acidic oxide (zirconia) favours complete reduction of hematite to metallic iron while on more neutral oxide (silica) hematite preferentially reduced through wüstite formation. The strong interaction between iron oxide and zirconia led to a shift to high temperature of the FeO reduction, very high activation energy values for this reduction were observed.

References

1 N. Hurst, S. J. Gentry, A. Jones and B. D. McNicol, Catal. Rev.-Sci. Eng., 24 (1982) 233.
2 S. Bhatia, J. Beltramini and D. D. Do, Catal. Today, 7 (1990) 309.
3 M. Fadoni and L. Lucarelli, Stud. Surf. Sci. Catal., Vol. 120A (Adsorption and its Applications in Industry and Environmental Protection, Vol. 1), Ed. A. Dabrowski, Elsevier, Amsterdam, 1999, pp. 177–225.
4 J. W. Jenkins, B. D. McNicol and S. D. Robertson, Chemtech, (1977) 316.
5 S. Subramanian, Platinum Metal Rev., 36 (1992) 98.
6 F. Kapteijn, J. A. Moulijn and A. Tarfaoui, Stud. Surf. Sci. Catal., Vol. 123 (Catalysis: an integrated approach), Elsevier, Amsterdam, pp. 525–541.
7 B. Jouguet, A. Gervasini and A. Auroux, Chem. Eng. Technol., 18 (1995) 243.
8 V. Boissel, S. Tahir and C. A. Koh, Appl. Catal. B, 64 (2006) 234.
9 F. J. Perez-Alonso, I. Melián-Cabrera, M. López Granados, F. Kapteijn and J. L. G. Fierro, J. Catal., 239 (2006) 340.
10 G. Neri, G. Rizzo, S. Galvagno, G. Loiacono, A. Donato, M. G. Mugolino, R. Pietropaolo and E. Rombi, Appl. Catal. A, 274 (2004) 243.
11 Y. Sun, S. Walspurger, J. P. Tessonnier, B. Louis and J. Sommer, Appl. Catal. A, 300 (2006) 1.
12 J. C. Groen, A. Brückner, E. Berrier, L. Maldonado, J. A. Moulijn and J. Pérez-Ramírez, J. Catal., 243 (2006) 212.
13 T. Nobukawa, M. Yoshida, K. Okumura, K. Tomishige and K. Kunimori, J. Catal., 229 (2005) 374.
14 M. Yoshida, T. Nobukawa, S. Ito, K. Tomishige and K. Kunimori, J. Catal., 223 (2004) 454.

15 F. Arena, G. Gatti, G. Martra, S. Coluccia, L. Stievano, L. Spadaro, P. Famulari and A. Parmaliana, J. Catal., 231 (2005) 365.
16 R. S. Prakasham, G. Sarala Devi, K. Raiya Laxmi and Ch. Subba Rao, J. Phys. Chem. C, 111 (2007) 3842.
17 A. Brăileanu, M. Răileanu, M. Crişan, D. Crişan, R. Bîrjega, V. E. Marinescu, J. Madarász and G. Pokol, J. Therm. Anal. Cal., 88 (2007) 163.
18 M. Ştefănescu, O. Ştefănescu, M. Stoia and C. Lazau, J. Therm. Anal. Cal., 88 (2007) 27.
19 S. Bennici, A. Auroux, C. Guimon and A. Gervasini, Chem. Mater., 18 (2006) 3641.
20 S. Bennici, A. Gervasini and V. Ragaini, Ultrason. Sonochem., 10 (2003) 61.
21 D. A. Monti and A. Baiker, J. Catal., 83 (1983) 323.
22 P. Malet and A. Caballero, J. Chem. Soc., Faraday Trans. I, 84 (1988) 2369.
23 A. Gervasini, C. Messi, A. Ponti and N. Ravasio, Nano Lett., submitted.
24 A. Pineau, N. Kanari and I. Gaballah, Thermochim. Acta, 447 (2006) 89.
25 E. E. Unmuth, L. H. Schwartz and J. B. Butt, J. Catal., 63 (1980) 404.
26 H.-Y. Lin, Y.-W. Chen and C. Li, Thermochim. Acta, 400 (2003) 61.
27 T. Herranz, S. Rojas, F. J. Pérez-Alonso, M. Ojeda, P. Terreros and J. L. G. Fierro, Appl. Catal. A, 308 (2006) 19.
28 K. Chen and Q. Yan, Appl. Catal. A., 158 (1997) 215.
29 H. Hayashi, L. Z. Chen, T. Tago, M. Kishida and K. Wakabayashi, Appl. Catal. A, 231 (2002) 81.
30 K. D. Chen, Y. N. Fan, Z. Hu and Q. J. Yan, Catal. Lett., 36 (1996) 139.
31 S. J. Gentry, N. W. Hurst, and A. Jones, J. Chem. Soc. Faraday Trans. I, 77 (1981) 603.
32 A. L. Boyce, S. R. Granville, P. A. Sermon and M. S. W. Vong, React. Kinet. Catal. Lett., 44 (1991) 1.
33 E. P. Barrett, L. G. Joyner and P. Halenda, J. Am. Chem. Soc., 73 (1951) 373.

DOI: 10.1007/s10973-007-8427-7